Auger-electron diffraction in the low kinetic-energy range: The Si(111)7×7 surface reconstruction and Ge/Si interface formation

M. De Crescenzi, R. Gunnella, R. Bernardini, M. De Marco, and I. Davoli
Dipartimento di Matematica e Fisica, Università di Camerino, 62032 Camerino, Italy
(Received 29 November 1994; revised manuscript received 22 February 1995)

We have investigated the Auger-electron diffraction (AED) of the $L_{2,3}VV$ Auger line of the clean 7×7 reconstructed Si(111) surface and the Ge/Si interface formed after a few monolayers (ML) of Ge deposition. The experimental AED in the low kinetic-energy regime has been interpreted within the framework of a multiple-scattering theory. The comparison of the AED data taken using both the x-ray source and an electron source evidences that the incident beam plays a negligible role when the experimental conditions require the use of an angular detector. The evolution of the Ge/Si(111) interface is studied by monitoring the intensity anisotropy of the Auger peaks of the two elements at room temperature (RT) and at 400 °C annealing temperature of the substrate. The evolution of the growth mechanism underlying the Ge/Si interface formation has been studied by exploiting the very low electron escape depth of this technique (≤ 5 Å). While at RT two monolayers of Ge deposition appear uniform and amorphous, the successive annealing induces an intermixing and a recrystallization only in the first two layers of the interface without any further interdiffusion. Furthermore, a Stranski-Krastanow growth mode has been deduced after deposition of 4 ML of Ge on a clean Si sample kept at 400 °C.

I. INTRODUCTION

Auger spectroscopy is the most currently used technique to obtain information on the chemical composition of surfaces and interfaces within a depth of a few atomic layers.[1] Furthermore, to obtain detailed information on the electronic properties of the investigated surface, the line shape of the Auger peak is analyzed in terms of filled density of states and correlation effects.[2–4] More recently this technique assumed a supplementary utility when the intensities of the Auger lines as a function of the polar and/or azimuth angle of the oriented sample are recorded in order to investigate the local-range order of surfaces.[5] The Auger peak angular anisotropy or Auger-electron diffraction (AED) has, essentially, the same origin as that accompanying the core-level photoemission diffraction spectra[5,6] (XPD). Simple kinematic-scattering theory can account for the observed anisotropy rather well at high kinetic energy. This gives rise, in the solid, to characteristic maxima along the directions with highest atomic density.[6,7]

Despite the great technological interest in silicon surfaces, very few XPD studies have been reported[8] and, within our knowledge, no AED experiments have been made in the low kinetic-energy range. The lack of experimental data on such a topic is probably due to the difficulty in defining a suitable model, which could account for the reconstruction occurring at the clean silicon surface during the preparation of the sample. In addition, the use of an electron source in AED is not completely assessed because of the unclear contribution of the incident-beam diffraction to the observed anisotropy. Concerning the last question we also report AED data for the Cu(100) in a polar-angle mode. The result of these measurements shows that the elastic peak (1500 eV) and the $L_{2,3}VV$ (918 eV) are strictly in-phase, while the $M_{2,3}VV$ (64 eV) results are completely in antiphase, as recently discussed after the analysis of XPD data.[9] In this way we demonstrate that, in our experimental conditions, incident-beam effects are negligible.

The aim of this work is to investigate—through the anisotropic intensities of the Auger $L_{2,3}VV$ line of the Si(111) surface–the 7×7 reconstructed surface, and the Ge/Si interface after a few monolayers of Ge deposition. The experimental data of the reconstructed surface are compared with a theoretical model based on a multiple-scattering approach as a function of several final-state angular momenta of the outgoing electrons. Theoretical simulation of the 1×1 (bulk-terminated) surface is compared with the 7×7 reconstruction of the Si(111) in terms of the DAS (dimer adatom stacking fault) model.[10] The small difference between the two calculations and between the simulations and the experimental data reveals the slight effect introduced by the 7×7 reconstruction on the AED data. AED measurements are important in order to confirm results obtained with those structural techniques, like low-energy electron diffraction (LEED) or scanning tunnel microscope (STM) which, although more sensitive to the structural details, do not have the chemical sensitivity that makes the AED at low kinetic energy particularly useful in the understanding of the early stages of the Ge/Si interface formation.

The paper is divided into seven sections including the introduction for an easier explanation of the work made. Section II describes the experimental setup of our AED experiment. Section III reports the formalism used in the computer simulation. Section IV is devoted to the discussion of the role played by the diffraction effects experienced by the incoming primary electron beam on the observed AED anisotropy features; then, Sec. V reports the $L_{2,3}VV$ Auger measurements performed on clean Si(111) and Sec. VI reports on the morphology of the Ge/Si(111)

0163-1829/95/52(3)/1806(10)/$06.00

©1995 The American Physical Society

interface, as a function of different thermal treatments of the substrate, for very thin overlayers. Finally, the conclusions are summarized in Sec. VII.

II. EXPERIMENT

The experiment was carried out in a UHV system equipped with a LEED and with a single-pass cylindrical mirror analyzer (CMA). LEED was used to check the long-range crystalline nature of the investigated surface and to correctly orient the surface. The CMA was modified to detect the angular dependence of the energy distribution of the outgoing electrons. A metallic screen was put in front of the analyzer to blind 354°/360° of the circular ring aperture. In this way, an angular detector having an acceptance of ±3° positioned at 42.6° from the primary electron-beam direction is obtained. A further description of the experimental apparatus is reported in Ref. 11. The use of a modified standard CMA as an angular electron detector in photoelectron diffraction experiments was originally adopted by Chambers and Swanson.[12]

The sample was an optically polished Si(111) crystal (p-type 0.1 Ω cm) clamped on two rods for direct joule heating. The atomic cleaning is obtained by a series of successive flashes at 1200 °C. To reach such a temperature, a current of about 8 A, flowing through the sample, was required. For the AED experiments we have used a primary electron beam of 1.5 keV and a peak-to-peak modulation of 0.5 V. The signal of the electron yield distribution was detected, by a lock-in amplifier, in the first-derivative mode $dN(E)/dE$. Figure 1 shows the Si $L_{2,3}VV$ Auger spectrum taken after the cleaning of the surface. Neither carbon nor oxygen were detected within the Auger atomic sensitivity. In this way, the degree of cleaning is estimated to be better than 0.5%. Furthermore, a sharp LEED pattern of the 7×7 reconstruction superimposed to the 1×1 bulk-terminated geometry was observed. This allows us to orient the sample according to the [$\bar{1}$10] direction. The inset of Fig. 1 shows the Auger spectrum of a Si(111) covered by a film of 3 Å of Ge (nominal thickness evaluated by a quartz microbalance) at room temperature (RT); such a thickness corresponds to about 2 ML. Along the [111] direction 1 ML equivalent to 7.83×10^{14} at/cm^2, corresponds to about 1.5 Å. For such a coverage, a first set of AED measurements have been performed monitoring both the Ge $M_{2,3}M_{4,5}M_{4,5}$ (51 eV) and the Si $L_{2,3}VV$ (92 eV) Auger transitions.

The effects of a different crystal orientation have been studied repeating the same polar-angle scan after an azimuth rotation of about 10°. We focused our attention on the polar-angle detection scan because this experimental mode is more sensitive than the azimuth-angle scan to the tetragonal strain effects, produced by the interface lattice mismatch, as demonstrated by Chambers and coworkers for the interfaces Ge/GaAs(100), Ge/Si(100),[13] and Cu/Ni(100).[14] A second set of AED measurements were performed after the 2-ML Ge/Si interface formed at RT followed by the annealing of the sample at 400 °C. Finally, a third set of measurements were made for a 4-ML Ge/Si interface prepared by keeping the Si substrate at 400 °C during the Ge evaporation. Sizable differences, induced by the three different procedures, were observed in the AED anisotropy.

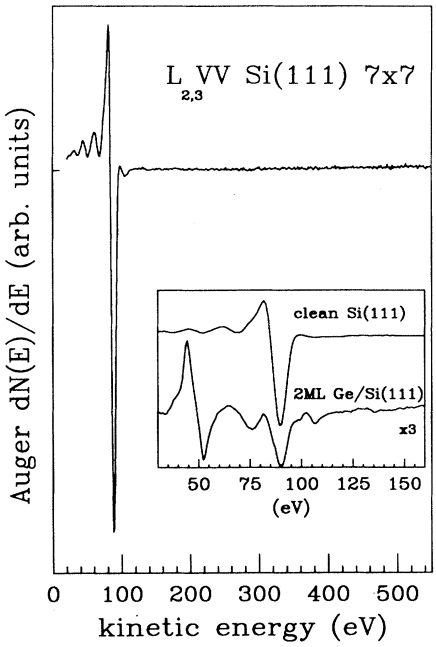

FIG. 1. Auger signal of the Si(111) 7×7 surface after a cleaning procedure described in the text. The inset shows the Auger signals due to 2 ML of germanium adsorbed on the clean silicon surface. The AED data are obtained using the Si $L_{2,3}VV$ (92 eV) and the Ge $M_{2,3}M_{4,5}M_{4,5}$ (51 eV) peaks.

III. THEORETICAL BACKGROUND

The importance of the electron-source wave is crucial to a full understanding of the anisotropy Auger spectra taken at kinetic energies below 300 eV. Indeed, a strong difference has been reported for Auger-electron diffraction compared to the corresponding XPS core-level diffraction.[9] Another matter of debate is the degree of localization of the source during Auger transition involving valence states.[1]

We performed theoretical calculations of the angular anisotropy of the Auger Si $L_{2,3}VV$ transition in the approximation of localization of the emission source. In fact, we have considered for silicon (a) the relatively high energy of the Auger transition involved due to the localized nature of the Si $2p$ core level and (b) the role played by both the Auger matrix element and the core-hole interaction to reduce the energy width of the line shape from the bandlike behavior of the Auger process to a quasiatomic behavior.[1,4,15]

The AED emission rate along a $\hat{k}$ direction can be written in the following way starting from the usual Fermi golden rule:[16]

$$\frac{dN}{d\hat{k}} = 2\pi \sum_{i,f} \left| \sum_{l,m} \sum_{j,l',m'} i^{-1} Y_{l',m'}(\hat{k}) \times A^{i,f}_{l,m} \tau^{o,j}_{l,m,l',m'} e^{-i\mathbf{k}\cdot\mathbf{R}_{j,0}} \right|^2 . \quad (1)$$

The first sum is done over all the initial and final states involved in the transition. In what follows, we neglect any selection rule concerning the initial magnetic quantum number operated by the direction of the incident electron beam. This effect should introduce not more than 5% of anisotropy.[17] In the above equation, j indicates the site index whereas "o" is the absorbing atom: $\mathbf{R}_{j0}$, is the difference vector $\mathbf{R}_j$-$\mathbf{R}_0$ between atomic coordinates. Y_{lm} are real spherical harmonics.

$\tau^{o,j}_{lm,l'm'}$ is defined as

$$\tau^{o,j}_{l,m,l',m'} = t^o_l - t^o_l G^{o,j}_{l,m,l',m'} t^j_{l'} + \sum_{k,l'',m''} t^o_l G^{o,k}_{l,ml'',m''} t^k_{l''} G^{kj}_{l'',m'',l'm'} t^j_{l'} - \cdots , \quad (2)$$

with t^j_l the complex atomic-scattering matrix evaluated as in Ref. 18 for atom i and wave l; $G^{ij}_{lml'm'}$ is a suitable propagator for the electron from site i to site j calculated within a spherical approximation as reported in Ref. 19 in the presence of a muffin-tin complex potential.

Equation (2) represents all the scattering events occurring during the process of electron emission: first- and higher-order scattering in the solid. As reported in the literature, multiple scattering is particularly important when emission is along low-indices crystallographic directions of the solid.[6] At low kinetic energy, the number of collinear atoms is greatly reduced by the low-electron mean free path in the solid. Furthermore, the use of a misorientation of the crystal of some degrees from the high atomic density rows makes us more confident about the validity of the approximation used. The calculation has been truncated to the second term in the above Eq. (2) and to the third term to test the second-scattering contribution. In doing this, we have found that when no more than two atoms are involved along one emission direction (referring to Figs. 5 and 7), the second-scattering perturbation is very small. The first-scattering series resulted in a better approximation of the full multiple-scattering series than the second-scattering approximation. This is due to the nonconvergence of the series, and the absence of successive order terms (third and fourth scattering), which introduce defocusing effects. On the basis of these considerations, we conclude that a single-scattering approximation constitutes a sufficiently accurate approach for the purposes of the present work.

In Eq. (1), $A^{i,f}_{l,m}$ represents the Auger matrix element where (l,m) is the angular momentum of the emitted electron. Evaluation of the matrix element would require cumbersome calculation. It is possible to take advantage of the angular-momentum conservation by the well-known triangular relation, for the case of states with (l_1, l_2, l_3) angular momenta participating to the Auger transition and a (l,m) emitted electron according to the following selection rules:[1,20,21]

$$|l_3 - |l_2 - l_1|| \le 1 \le l_3 + l_2 + l_1 ,$$
$$l_3 + l_2 + l_1 + 1 = (\text{even}) , \quad (3)$$
$$m_1 + m_3 = m_2 + m .$$

In the $L_{2,3}VV$ transition of Si, the dominant character p-p of the symmetry of the two valence-band electrons[1,4,15] implies the presence of channels with final states $l=1$ and $l=3$ with an intensity ratio of 19/27. Furthermore, fit calculations have been performed for different l and the best result has been found for angular momentum $l=3$.

We show, in Fig. 2, the calculation of four possible final states for emitted Auger electron. Note that the $l=1$ (p character) has a negligible contribution to the anisotropy while all the other curves show a relative maximum at 0° polar-angle emission. Contrary to what was found for the Cu $M_{2,3}VV$ Auger anisotropy,[9] where a dip in the intensity at 0° emission is observed, in silicon the initial p valence state seems not to affect the main features due to the crystallographic structure. The same strong dependence on the emission channel has not been found in the AED for the Si KLL transition (not shown in the present paper) where all the different channels give rise to the same kind of anisotropy of the AED data.

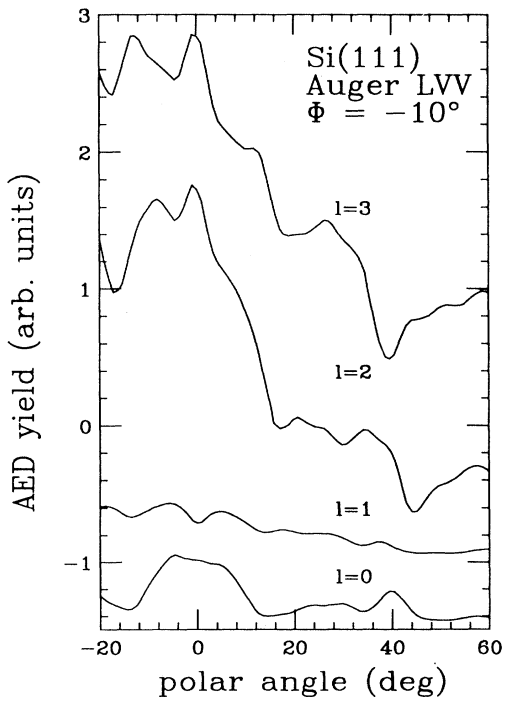

FIG. 2. Theoretical calculation of AED polar scan for four l channels of the outgoing Auger electron of the Si(111) surface in the approximation of single scattering and a kinetic energy of 95 eV.

IV. INCIDENT BEAM EFFECTS

The real influence of the electron primary beam diffraction in AED experiments and the assessment of AED as a structural technique has been a matter of debate within the surface-science community. Indeed, some major effects due to the primary beam excitation mechanism were singled out by several authors.[22] They put emphasis on suitable experimental geometries to separate the incident-beam diffraction from the genuine outgoing electron-diffraction effects. On the other hand, many evidences are also present in literature about the independence of the excitation mechanism in AED experiments. Chambers *et al.*[23] using several angles of incidence of the electron primary beam concluded that incident-beam diffraction was a second-order effect. Furthermore, comparison of the electron-excited experiments[23] with x-ray-excited Auger diffraction[24] showed the same polar-angle anisotropies. On the basis of these considerations, it is difficult to give a general rule on the degree of influence of primary electron diffraction in AED. It has been demonstrated by De Crescenzi *et al.*[25] that the calculation of the inelastic cross section presents complex aspects involving a strong coupling between loss mechanism and diffraction events, which depends both on the electronic and structural properties of the solid. First AED experiments on CVV (core-valence-valence) low-kinetic-energy Auger transition were performed by White, Woodruff, and McDonnell.[26] The interplay between delocalization, anisotropy of the Auger-electron final state, and multiple scattering of the outgoing electron has been discussed. In that paper an f-like wave is emitted from each localized atomic site and the kinetic energy is high enough to allow a single-scattering approximation.

To prove that incident-beam diffraction effects are negligible compared to the genuine diffraction experienced by the outgoing electrons, we measured the polar-angle anisotropy of the elastic peak, the $L_{2,3}M_{4,5}M_{4,5}$ (918 eV), and $M_{2,3}M_{4,5}M_{4,5}$ (64 eV) of Cu(100) surface along the [100] direction. The data reported in Fig. 3 show that, even though the *LMM* are on-phase with the elastic peak, the *MMM* spectrum is in antiphase. Particularly at 0° polar emission angle, *LMM* spectrum shows a maximum while the *MMM* spectrum has a minimum. These data are in good agreement with those reported by Greber *et al.*, who investigated the same surface by means of an x-ray source in a 2π scan[9] and with the calculation performed by Chen, Harp, and Saldin.[21] The clear antiphase effect noted between the *LMM* and *MMM* excludes any appreciable incident-beam diffraction contribution to the intensity anisotropy. Different conclusions are reported by Valeri and co-workers.[27] Indeed they observed sizable incident-beam diffraction effects using a standard CMA analyzer not screened as in our experimental conditions. Operating with an integrated analyzer, a complete average of the outgoing diffraction events occurs and the anisotropy observed is due to the incident electron beam. Furthermore, the measured signal modulation was independent on the kinetic energy of the collected electrons.

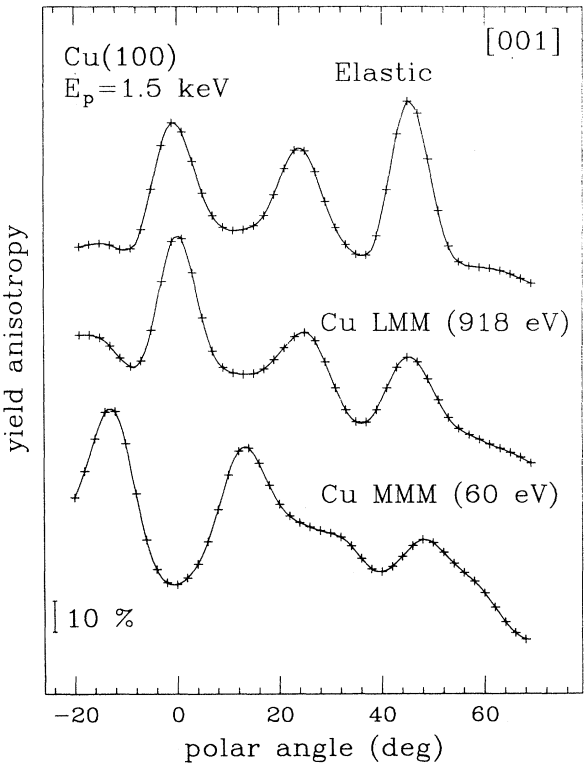

FIG. 3. Cu(100) surface polar-angle anisotropy obtained for the elastic (1500 eV), *LMM* (918 eV), and *MMM* (64 eV) Auger structure.

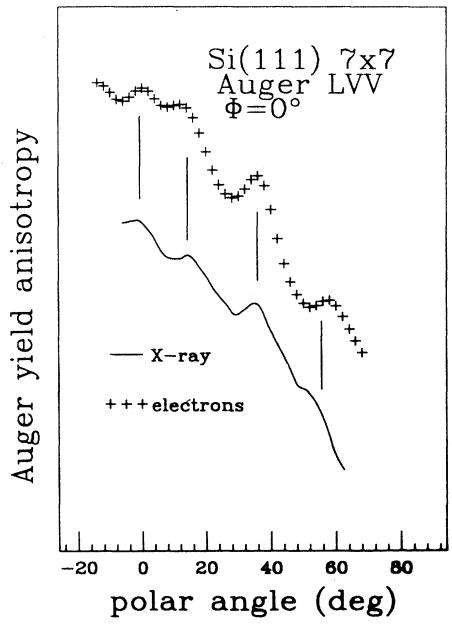

FIG. 4. Comparison between AED polar scan of clean Si(111) 7×7 surface along [$\bar{1}$10] direction of two independent experiments using a primary electrons beam (crossed line) and x-ray excitation (solid line) for the Si $L_{2,3}VV$.

On the basis of our experimental results, we conclude that incident-beam effects become appreciable only when the electron analyzer acts as an integrated one. Further evidence of the complete independence of AED from the excitation source is given in Fig. 4 where the Auger signal excited by means of x rays is compared with the experimental data of the same Auger signal detected from the same surface using an electron gun. Both features of the angular anisotropy and their intensities constitute convincing evidence of the limited relevance of the primary beam diffraction effects when the outgoing electrons are detected by an angle-resolved analyzer.

V. CLEAN Si(111) 7×7 SURFACE

In Fig. 5 we show the raw Auger-electron diffraction data for the clean Si(111)7×7 surface compared with theoretical calculations. The experiment is performed along the [1̄10] azimuth direction.[8] The angles are measured from the normal to the surface. The experimental data have not been corrected by any instrumental response function although this has been estimated to have a trend following the $\cos\theta/\cos(42°-\theta)$ function, where θ is the polar angle which will be considered also with its negative values referring to the sample normal. The factor $\cos(42°-\theta)$ accounts for the angle between the electron source and the CMA aperture. Because of the finite size of the primary electron beam and of the electron escape depth, the portion of solid that contributes to the emission process decreases with θ giving the characteristic behavior. Each dot is the measure of the peak-to-peak Auger line electron yield detected in the first-derivative mode $dN(E)/dE$. Such an experimental method was demonstrated to have the same angular behavior as the one obtained by measuring the area under the Auger line transition in the $N(E)$ spectrum.[22] In Fig. 6 are reported the sketches of the reconstructed Si(111)7×7 surface and the plane normal to the surface along the [1̄10] direction. The unfaulted and the faulted sequence of the surface geometry are reported in Figs. 6(a) and 6(b), respectively. These sketches give particular prominence to the atomic planes involved in the scattering events. The planes are not equivalent and are all needed to correctly explain AED data. Indeed the internuclear pathways involving coplanar atoms are indicated and occur at the same angles of features *A*, *C*, and *D* of Fig. 5. Feature *B*, which has no correspondent forward-scattering pathway, might be attributed to the spherical

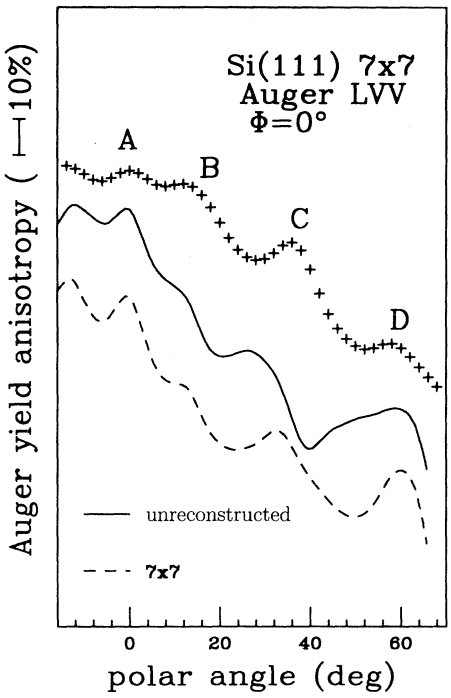

FIG. 5. Si(111) $L_{2,3}VV$ AED polar-angle data obtained for a 7×7 surface oriented along the direction [1̄10]. The theoretical calculations are made for a bulk-terminated surface (solid line) and for a 7×7 reconstructed surface (dashed line) according to the DAS model (Ref. 10). The features labeled *A*,*C*,*D* correspond to the most prominent scattering pathways as shown in Fig. 6.

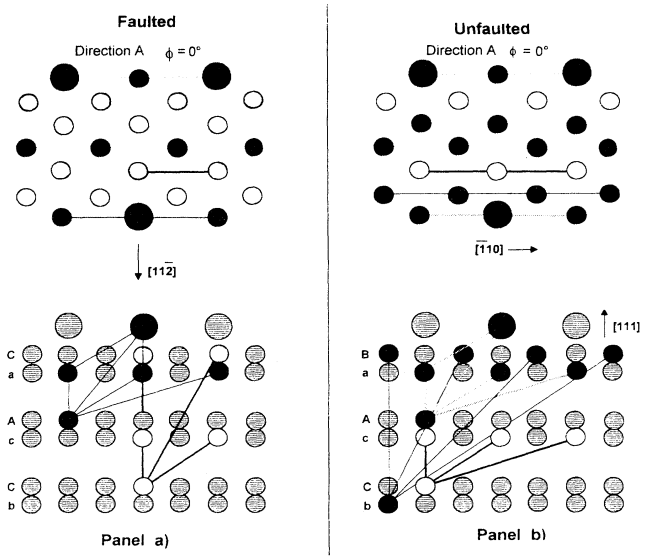

FIG. 6. Schematic view of the Si(111) 7×7 surface. The upper part of panel (a) shows the top view of the 7×7 faulted reconstruction where the adatoms are represented as large black balls. The direction [1̄10] and the direction [11̄2] are reported as *x* axis and *y* axis, respectively. In the lower part of panel (a) is shown a sideview of the six top layers plus the adatom layer probed by the electron escape depth in our experiment. The figure shows the possible scattering pathways due to inequivalent planes perpendicular to the surface. All the pathways traced contribute to the AED spectra. The letters label the faulted stacking sequence $(bCcA)aB$ according to the DAS model Ref. 10. The gray balls represent the bulk lattice atoms beyond the selected planes. The first atomic layer (C) is rotated 60° with respect to the unfaulted case. Panel (b) is the same as (a) for the unfaulted case. In this case the stacking sequence is $(bcCA)a/B$. Grays of atoms follow the stacking sequence of the planes.

nature of the scattering amplitude for the kinetic energy used in our experiment.

The solid and the dashed curves in Fig. 5 are the theoretical calculations: The solid curve is obtained considering a model built by six layers of a bulk-terminated Si(111) surface. The layers involved were sufficient to account for the 5-Å escape depth of the electrons having about 100-eV kinetic energy.[28] The dashed curve in Fig. 5, is a theoretical calculation of a cluster made of six layers with the two top layers reconstructed by means of a simplified version of the 7×7 as reported by Takayanagi *et al.* in terms of the DAS model.[10] This implies adatoms on the two triangular subunits characterized by a different stacking sequence (unfaulted and faulted) as reported in Fig. 6. In this model we neglect any dimerization effect at the boundaries of the triangular units. The experimental features *A*, *B*, and *D* are well reproduced by both theoretical models; feature *C* seems to be better reproduced by the model, which accounts also for the reconstructed adatom layer. To study the effect of a different atomic alignment, in Fig. 7 are reported the same polar-angle measurements of Fig. 5 after an azimuth rotation of −10°. The solid and dashed curves of Fig. 7 report the theoretical calculation for the bulk-terminated and for the 7×7 reconstructed surface. The internuclear directions that contribute to forward-scattering events are indicated in Fig. 8. Even in this case, the reconstructed model better reproduces the experimental data.

One of the goals of our experiment was to single out the reconstruction effect on the AED data for low

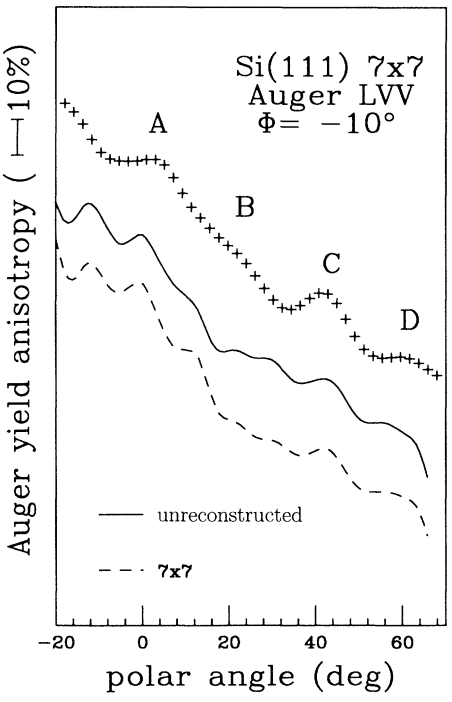

FIG. 7. Same as in Fig. 5. The AED measurements and the theoretical calculations are performed for a surface geometry rotated by an azimuth angle of −10° with respect to the [1̄10] direction.

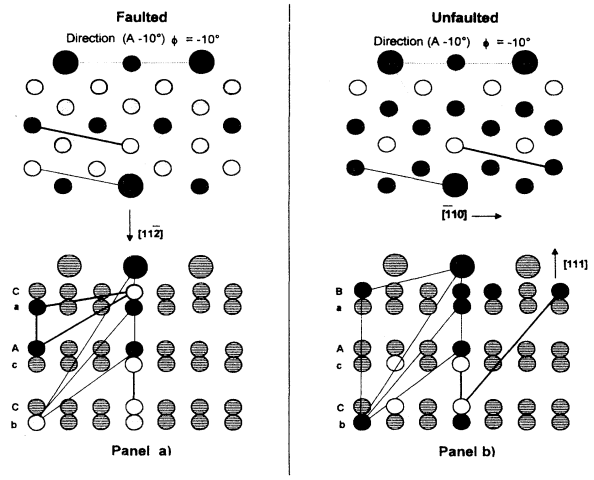

FIG. 8. Same model as described in Fig. 6. The planes indicated are those intercepted by an azimuth rotation of −10° with respect to the [1̄10] direction. In the lower figures, the lines between atoms indicate the possible scattering pathways involving atoms of the first six layers probed in our experiment.

kinetic-energy Auger transition. We note that there are only minor differences between the two theoretical curves reported both in Fig. 5 and in Fig. 7. This suggests that the surface reconstruction does not introduce, clearly detectable, additional features different from those of the bulk-terminated surface, even if the electron escape depth is the most superficial one. The negligible effect induced by the surface reconstruction is interpreted as due to the reduced contribution of the first two layers (adatoms and first full layer) when compared with the remaining five atomic planes used in the calculation. This is also clear in Fig. 9 where the different contributions from the whole

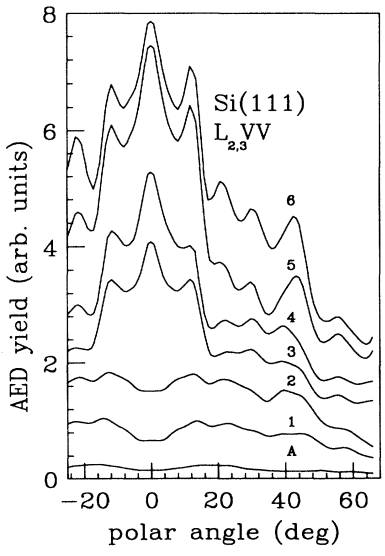

FIG. 9. Theoretical calculations of AED spectra involving different silicon layers calculated for $l=3$. Bottom curve *A* is due to the adatoms contribution. For the other curves, the numbers indicate the sum of the *n*th layer plus all the previous ones.

cluster are reported. On the very bottom, the curve *A* represents the adatoms contribution, which has a negligible effect on the features of the entire slab. Going from the bottom to the top, the curves reported in the figure are the result of the *i*th atomic plane plus all the previous deeper layers. Enough sensitivity to the surface reconstruction could be achieved by a better energy-resolved experiment and by means of surface core-level shift photoelectron diffraction measurement in order to select photoemission from the very first atomic layers as demonstrated by Gota *et al.*[29] Our results are in agreement with XPD data reported in a recent paper by Seelmann-Eggebert *et al.*[30] The authors observed that on CdTe(110) and on GaAs(100) the assessing of surface reconstruction is rather limited by the electron mean free path and by the defocusing and the randomization caused by multiple-elastic scattering. These effects are sufficiently sizeable to reduce the necessary surface sensitivity even in the case of the reconstruction involving one atom over two per unit cell and in the case of surface relaxation.[31]

VI. Ge/Si(111) INTERFACE

The study of the Ge growth on the Si substrate is mainly driven by the remarkable development of the electronic and optoelectronic technology.[32] Such an interest is at the present mostly devoted to the (100) surface due to the wide diffusion of this surface for industrial applications. Nevertheless, efforts in the study of the (111) surface received considerable attention because strained and perfect Ge films can be grown on Si(111) with a reduced number of dislocations, which is essential to obtain any type of multilayers.[33] A number of electronic and structural techniques has been employed to clarify the structure and the growth mechanism of the Ge layers.[34] Because of the lattice mismatch, the growth morphology is expected to critically depend on the thermodynamic conditions and on the reconstruction details.

The present work reports on Auger-electron diffraction following the growth of a few monolayers of germanium on the Si(111) substrate in order to check the most accepted growing models reported in literature.[35] The photoelectron diffraction technique has been used in the past by Chambers and Loebs[13] and by Diani *et al.*,[36] who have studied the Si(100) surface covered by Ge layers using $2p$ and $3d$ core-level transitions in the XPD technique. Thus, we may consider the present work as the first structural study of the Ge/Si(111) interface using AED at very low kinetic energy. The full morphology of this interface at its early stage of formation is still a matter of debate. Indeed previous LEED data suggested no intermixing[36,37] while reflection high-energy electron-diffraction (RHEED) studies reported by Shinoda *et al.*[38] have revealed an intermixing effect for a film deposition occurring at $T \geq 300\,^{\circ}\mathrm{C}$. Furthermore, a great indetermination exists in assessing the true morphology at the interface induced by the strain and by the dislocation during the interface formation. To distinguish among all the possible interface configurations is a real puzzle, because a great number of models have the same probability to minimize the total energy of the surface.[39] It has been shown that thickness effects of the deposited Ge plays a very critical role. For a coverage less than 6 ML, the Ge atoms can easily intermix and exchange their positions with the Si substrate. While for thicker coverage, exchange of Ge with Si rarely occurs favoring a three-dimensional (3D) Ge-islands formation.[40] Strong deviation from the ideal layer-by-layer growth implies a reduction of the direct band gap created by the zone folding in superlattices devices.[32]

In Fig. 10 we report AED data for Ge/Si(111) interface deposited at RT. In Fig. 10, the Si $L_{2,3}VV$ line of the clean Si(111) is compared with the Ge $M_{2,3}M_{4,5}M_{4,5}$ line of the system formed by 2 ML of Ge deposited on the clean substrate. Since the experimental Auger signals have almost the same kinetic energy (51 and 91 eV), the structural AED information is expected to be referred to the same number of superficial layers. We observe that the anisotropy of the Si $L_{2,3}VV$ detected after the germanium deposition (curve *b*) has peaks in the same polar-angle position with reduced intensity if compared to the features of the clean Si surface (curve *a*). On the contrary, the germanium AED anisotropy (curve *c*) does not have any significant structure in addition to the instrumental response function. This indicates that at RT the germanium deposition forms a uniform and amorphous film without apparent interdiffusion. We arrive at a similar conclusion by analyzing the data taken along a direction rotated of an angle of $-10°$ with respect to the $[\bar{1}10]$ direction (see Fig. 11). Our data agree with the RHEED data of Shinoda *et al.*,[38] who recently measured the structural changes of the initial growth of Ge/Si(111).

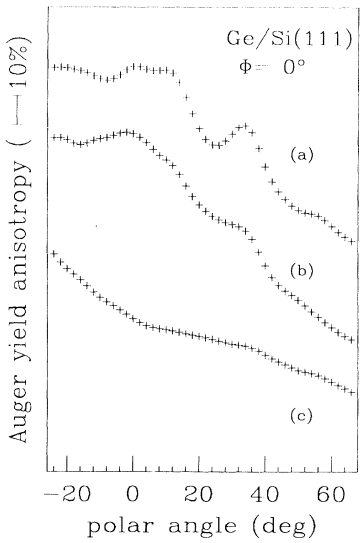

FIG. 10. Comparison of the AED data for a clean Si(111)7×7 surface and for a 2 ML of Ge deposited at RT. Top curve (a) is the polar scan of the Si $L_{2,3}VV$ along the direction $[\bar{1}10]$ of the clean surface. The others two curves (b) and (c) are obtained after the Ge deposition. The medium curve is collected from the Si $L_{2,3}$ of the substrate while the lower curve is due to the Ge $M_{2,3}M_{4,5}M_{4,5}$ Auger line.

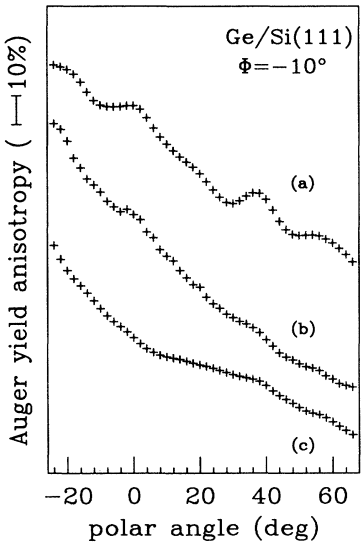

FIG. 11. Same polar AED data as shown in Fig. 10 obtained after a rotation of the azimuth angle of −10°. Curve (a) is the clean Si surface while curves (b) and (c) are obtained after 2-ML Ge deposition monitoring the Auger Si substrate and the Ge signal, respectively.

In Fig. 12, the change of the AED data for the silicon substrate heated up to the temperature of 400 °C for 10 min is reported. We note that the AED Si signal detected after the annealing (curve *b*) resembles very closely the clean Si $L_{2,3}VV$ signal (curve *a*) because the features measured at 0° and at 40° are more enhanced with respect to the anisotropy reported on curve *b* of the previous figure. Furthermore, the signal due to the germanium (curve *c*) shows a marked structure at about 40° and few other features but no structure at all at 0°. The appearance of well-defined features on both curves is an indication of a crystalline intermixing. Indeed the formation of a continuous Ge crystalline layer would strongly attenuate the anisotropy features of the Si substrate, while the experiment does not show any attenuation. We verified that also in the case of the Ge *MMM* AED the predominance of the $l=3$ channel for the outgoing electron leads to angular patterns very similar to those relative to the Si $L_{2,3}VV$ reported in Fig. 9. Thus, the growing of the continuous layers of Ge on Si should have the same trend as that reported in Fig. 9. This means that only after the complete formation of the third layer, we may observe the prominent peak located at 0° emission angle. In the reaction region, the Ge atoms substitute the Si atoms in the crystalline lattice. This is evidenced by the similarity of curve *b* with curve *a* of Fig. 12.

The systematic LEED inspection performed during all the phases of the surface preparation showed the presence of the 5×5 pattern. This characteristic reconstruction has been studied by Becker, Golovchenko, and Swartzentruber[41] and in great detail by Kajiyama, Tanishiro, and Takayanagi.[42] They demonstrated that the 5×5 DAS structure is stabilized by Ge. The sites of the adatoms and of the underlying layers are occupied partially by Ge atoms. The migration of the Ge atoms into the Si matrix allows the floating of Si atoms in an ordered fashion. An agglomerated phase of Ge on the Si substrate is not justified on the basis of our results. In this condition, the Ge film leaving a large part of the substrate uncovered, would justify the persistence of curve *b*, but certainly not the AED spectrum shown in curve *c*. In fact because of the misoriented nature of the Ge clusters, no structures on curve *c* should appear. The latter is evidenced by several STM pictures of clusters deposited on semiconductors where no ordered growth mode has been reported.[43] The coupled analysis of the Ge and Si AED data supports an intermixing of the Ge atoms into the Si

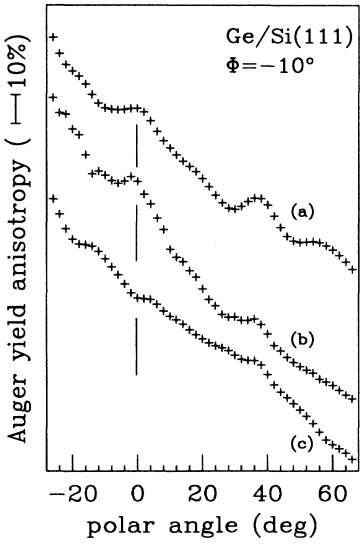

FIG. 12. Polar AED data as shown in Fig. 11 obtained after annealing of the silicon substrate up to 400 °C for 10 min.

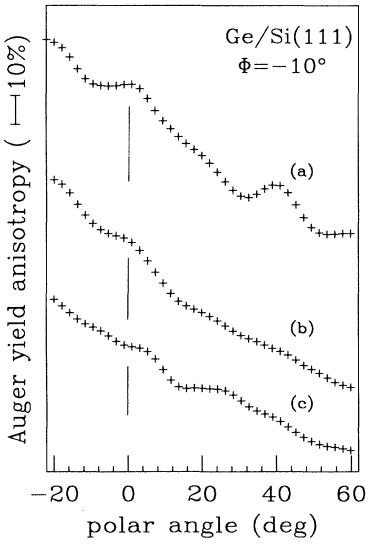

FIG. 13. Polar AED data as shown in Fig. 12 obtained after 2 ML of germanium evaporated on Si(111) kept at 400 °C.

substrate.[39] The interface reaction region is limited to the first two layers without any further interdiffusion.[40]

Finally, Fig. 13 shows the comparison of the AED data obtained for 4 ML of germanium evaporated on Si(111) substrate kept at 400 °C to favor recrystallization conditions at the interface. For such a procedure, a Stranski-Krastanow (SK) growing mode is expected to occur, i.e., the formation of a first continuous Ge layer followed by 3D islands formation.[42,43] This growing mode is suggested by the slightly smoothed AED signal shown in curve *b*, which has all the structures in the same position of the clean silicon AED (curve *a*), while the anisotropy of the Ge signal (curve *c*) does not show the 0° structure. The absence of any structure at 0° can be interpreted, on the basis of the theoretical curves shown in Fig. 9, as the absence of any germanium interdiffusion into the substrate. Indeed, the formation of an alloy due to an interdiffusion would favor a Ge and Si anisotropy signal very similar to each other. The formation of a one or two laminar Ge layers followed by the typical clusterization of the SK structure is strongly suggested by the present AED signals.

VII. CONCLUSIONS

We have reported polar-angle AED data of Si $L_{2,3}VV$ with the aim of investigate the role of the 7×7 surface reconstruction. This is done by comparing the experimental AED data with a multiple-scattering calculation taking into account both the reconstruction and the six bulk layers probed with our technique. Incident-beam effects were negligible in the present experimental setup and we support the use of primary electron diffraction AED to investigate surface morphologies. In fact, even if this technique is not sufficiently sensitive to yield the full geometry of such a reconstruction, its atomic selectivity allows us to follow the process occurring at the interface. For 2 ML of Ge deposited on clean Si substrate and after an annealing up to 400 °C, we may deduce the occurrence of intermixing and recrystallization at the interface. The diffusion length of the intermixing being limited to 2 ML supports the existence of a critical thickness above which the annealing of the silicon substrate should produce Ge islands. Indication of a SK growth mode for 4-ML Ge deposition may be deduced by the lack of Ge features. A SK growth mode yields a sizable attenuation of the electron emission from the Si substrate.

ACKNOWLEDGMENTS

The authors are indebted with Dr. C. R. Natoli and Dr. A. Di Cicco for valuable discussions and suggestions. Technical support of F. Bizzarri is greatly acknowledged. This work was partially supported by the European Human Capital and Mobility Contract No. CHRX-CT93-0355.

[1]R. Weissmann and K. Müller, Surf. Sci. Rep. **105**, 251 (1981).
[2]P. A. Bennet, J. C. Fuggle, F. U. Hillebrechet, A. Lenselink, and G. A. Sawatzky, Phys. Rev. B **27**, 2194 (1983).
[3]M. Cini, Solid State Commun. **24**, 681 (1977); Phys. Rev. B **17**, 2788 (1978).
[4]D. E. Ramaker, F. L. Hutson, N. H. Turner, and W. N. Mei, Phys. Rev. B **33**, 2574 (1986).
[5]S. A. Chambers, Surf. Sci. Rep. **16**, 261 (1992), and references therein.
[6]C. S. Fadley, in *Progress in Surface Science,* edited by S. G. Davison (Pergamon, New York, 1984); *Synchrotron Radiation Research: Advances in Surface Science,* edited by R. Z. Bachrach (Plenum, New York, 1990).
[7]W. F. Egelhoff, Jr., Phys. Rev. Lett. **59**, 559 (1987).
[8]J. L. Bischoff, L. Kubler, F. Lutz, M. Diani, and D. Bolmont, Solid State Commun. **83**, 823 (1992); L. Kubler, F. Lutz, J. L. Bischoff, and D. Bolmot, Surf. Sci. **251/252**, 305 (1991).
[9]L. J. Terminello and J. J. Barton, Science **251**, 1281 (1991); T. Greber, J. Osterwalder, D. Naumovic, A. Stuck, S. Hufner, and L. Schlapbach, Phys. Rev. Lett. **69**, 1947 (1992).
[10]K. Takayanagi, Y. Tanishiro, M. Takahashi, and S. Takahashi, J. Vac. Sci. Technol. A **3**, 1502 (1985); G. X. Qian and D. J. Chadi, Phys. Rev. B **35**, 1288 (1987).
[11]I. Davoli, R. Bernardini, C. Battistoni, P. Castrucci, R. Gunnella, and M. De Crescenzi, Surf. Sci. **306**, 144 (1994).
[12]S. A. Chambers and L. W. Swanson, Surf. Sci. **131**, 385 (1983).
[13]S. A. Chambers and V. A. Loebs, Phys. Rev. Lett. **63**, 640 (1989); Phys. Rev. B **63**, 640 (1989); **42**, 5109 (1990).
[14]S. A. Chambers, H. W. Chen, I. M. Vitomirov, S. B. Anderson, and J. H. Weaver, Phys. Rev. B **33**, 8810 (1986).
[15]K. C. Pandey, Phys. Rev. B **14**, 1577 (1976).
[16]C. R. Natoli, M. Benfatto, C. Brouder, M. F. Ruiz Lopez, and D. L. Foulis, Phys. Rev. B **42**, 1944 (1990).
[17]B. Cleff and W. Mehlorn, J. Phys. B **7**, 593 (1974).
[18]T. A. Tyson, K. O. Hodgson, C. R. Natoli, and M. Benfatto, Phys. Rev. B **46**, 5997 (1992).
[19]J. Mustre de Leon, J. J. Rehr, C. R. Natoli, C. S. Fadley, and J. Osterwalder, Phys. Rev. B **39**, 5632 (1989).
[20]E. U. Condon and C. H. Shortley, *The Theory of Atomic Spectra* (Cambridge University Press, Cambridge, England, 1979).
[21]X. Chen, G. R. Harp, and D. K. Saldin, J. Vac. Sci. Technol. A **12**, 428 (1994).
[22]Y. U. Idzerda and G. A. Prinz, Phys. Rev. B **43**, 11 460 (1991); H. E. Bishop, B. Choruik, C. Le Gressus, and A. Le Moel, Surf. Interface Anal. **6**, 116 (1984).
[23]S. A. Chambers, H. W. Chen, S. B. Anderson, and J. H. Weaver, Phys. Rev. B **34**, 3055 (1986).
[24]Z. L. Han, S. Hardcastle, G. R. Harp, H. Li, X-D. Wang, J. Zhang, and B. P. Tonner, Surf. Sci. **258**, 313 (1991).
[25]M. De Crescenzi, L. Lozzi, P. Picozzi, S. Santucci, M. Benfatto, and C. R. Natoli, Phys. Rev. B **39**, 8409 (1989).
[26]S. J. White, D. P. Woodruff, and L. McDonnell, Surf. Sci. **72**, 77 (1978).
[27]S. Valeri and A. di Bona, Surf. Sci. Lett. **289**, L617 (1993); S. Valeri, A. di Bona, and G. C. Gazzadi, Surf. Sci. **311**, 422 (1994).
[28]A. Di Cicco, A. Bianconi, and N. V. Pavel, Solid State Commun. **61**, 635 (1987).
[29]S. Gota, R. Gunnella, Z. Y. Wu, G. Jezequel, C. R. Natoli, D. Sebilleau, E. L. Bullock, F. Proix, C. Guillot, and A. Quem-

erais, Phys. Rev. Lett. **71**, 3387 (1993).

[30]M. Seelmann-Eggebert, R. Klauser, G. P. Carey, E. C. Larkins, P. Meisen, and H. J. Richter, in *The Structure of Surfaces IV,* edited by X. Xie, S. Y. Tong, and M. A. Van Hove (World Scientific, Singapore, 1994).

[31]Shika Varma, X. Chen, J. Zhang, I. Davoli, D. K. Saldin, and B. P. Tonner, Surf. Sci. **314**, 145 (1994).

[32]H. Presting, H. Kibbel, M. Jaros, R. M. Turtou, U. Menczigar, G. Abstreiter, and H. G. Grimmeiss, Semicond. Sci. Technol. **7**, 1127 (1992), and references therein.

[33]M. Horn-von Hoege, F. K. LeGoues, M. Copel, and R. Tromp, Phys. Rev. Lett. **67**, 1130 (1991); F. K. LeGoues, M. Horn-von Hoege, M. Copel, and R. Tromp, Phys. Rev. B **44**, 12 894 (1991).

[34]M. A. Herman and H. Sitter, in *Molecular Beam Epitaxy* (Springer-Verlag, Berlin, 1989).

[35]P. M. J. Maree', K. Nakagawa, F. M. Mulders, J. F. Van der Veen, and K. L. Kavanagh, Surf. Sci. **191**, 305 (1987).

[36]M. Diani, D. Aubel, J. L. Bishoff, L. Kubler, and D. Bolmont, Surf. Sci. **291**, 110 (1993).

[37]K. Shoji, M. Hyodo, H. Ueba, and C. Tatsuyama, Jpn. J. Appl. Phys. **22**, 1482 (1983).

[38]Y. Shinoda, N. Shimizu, H. Hibino, T. Nishioka, C. Heimlich, Y. Kobayashi, S. Ishizawa, K. Sugii, and M. Seki, Appl. Surf. Sci. **60/61**, 112 (1992), and references therein.

[39]D. E. Jesson, S. J. Pennycook, and J.-M. Baribeau, Phys. Rev. Lett. **66**, 750 (1991).

[40]T. Ichikawa and S. Ino, Surf. Sci. **136**, 894 (1984).

[41]R. S. Becker, J. A. Golovchenko, and B. S. Swartzentruber, Phys. Rev. B **32**, 8455 (1985).

[42]K. Kajiyama, Y. Tanishiro, and K. Takayanagi, Surf. Sci. **222**, 47 (1989).

[43]R. M. Feenstra, Phys. Rev. Lett. **63**, 1412 (1989); Surf. Sci. **56**, 104 (1992); B. M. Trafas, Y.-N. Yang, R. L. Siefert, and J. H. Weaver, Phys. Rev. B **43**, 14 107 (1991).